THE PUBLISHING HOUSE
OF THE ROMANIAN ACADEMY

PROCEEDINGS OF THE ROMANIAN ACADEMY, Series A,
Volume 9, Number 1/2008, pp. 000–000

ON THE FURLING MECHANISM FOR POWER REGULATION

Horia DUMITRESCU[*], Alexandru DUMITRACHE *, Vladimir CARDOŞ[*]

[*] Institute of Mathematical Statistics and Applied Mathematics
Corresponding author: Horia DUMITRESCU, e-mail: horiad12@yahoo.com

Stall control and pitch control are the most commonly used methods of regulating power. However, through the opportunities presented by the flexible (or teetered) hub of a two-bladed teetered rotor one can also utilize yaw control to regulate power. This is achieved by adjusting the capture area of the rotor disk relative to the prevailing wind direction. This paper presents the aerodynamic and aeroacoustic results obtained from theoretical models for such a rotor when is yawed to the undisturbed flow. The non-axial flow operating conditions results in a variation in the power output and noise spectrum. Some comparisons between calculated and measured noise spectra of a yaw controlled wind turbine show good agreement over all angles up to 60 degrees of yaw.

Key words: Aerodynamics; Aeroacoustics, Unsteady flow; Wind turbines, Rotor vortex wake.

1. INTRODUCTION

Modern in utility-sized wind turbines rely mainly on two mechanisms for power control at high wind speeds, namely pitch and stall control [1-3]. Pitch control relies on an active full-span variation of the global blade angle, thereby guaranteeing that all sections of the blade remain in a regime which can be characterized by mostly unseparated flow around the blade. A theoretical description in this regime can be performed by essentially inviscid flow models, yielding reliable results for the local lifting forces and the overall torque developed by the blade. Drag forces are negligible in this regime.

Stall control, on the other hand, operates in an aerodynamic regime, characterized by local flow separation and strong drag forces. An adequate theoretical description requires a solution of the full equations of viscous motion, which is impractical in most cases; therefore a number of semi-empirical models has been developed but which have to be adjusted manually to the exact blade parameters and conditions. Pitch-controlled wind turbines can operate at both fixed and variable rotor frequency, whereas stall control heavily relies on a fixed rotor frequency.

Small wind turbines, with rated power values in the $0.5-20$ kW range, however, mainly utilize furling (or yawing) as their mechanism for power regulations. This is achieved by adjusting the capture area of the rotor disk relative to the dominant wind direction. Although, yaw control is a robust and well-suited mechanism for its typical applications (water pumping, rural electrification) at medium wind speed, the non-axial flow results in a poor performance at higher wind speeds and may create serious resonances in the blade or supporting structure and modifications of the noise spectrum.

In the present work a modified strip theory approach has been used to determine the effects of non-axial flow on the power performance and sound pressure level.

2. AERODYNAMIC ANALYSIS

Blade element momentum (BEM) theory is the standard computational technique for the prediction of power curves of wind turbines; it is based on the two-dimensional aerodynamic characteristics of airfoil blade elements and some corrections accounting for three-dimensional wing aerodynamics. Before being

able to calculate the force and moments on a blade, it is necessary to derive the velocity components of the air flow relative to any point on the blade and also the induced velocity components.

2.1 Velocity Components at the Blade

The following analysis has been applied to upwind horizontal axis turbine as shown in Fig. 1.

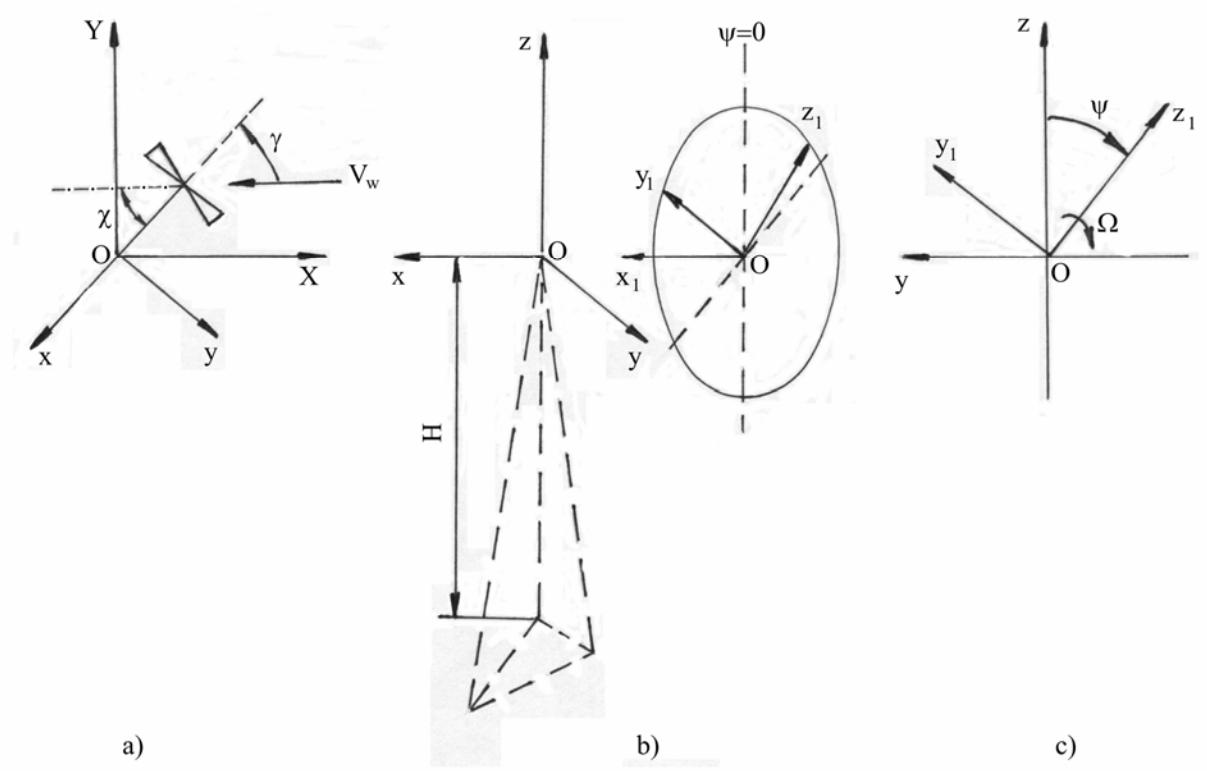

Fig. 1 Coordinate systems describing wind turbine: a) (*X,Y,Z*) - ground based coordinates; b) (*x,y,z*) - rotor based coordinates; c) (x_1, y_1, z_1) - blade based coordinates.

The final reference frame is a set of orthogonal axes fixed relative to the blade such that the z_1 axis is along the span, y_1, in the direction of rotation and x_1 being perpendicular to y_1 and z_1 (the rotor plane).

The undisturbed flow can be expressed in the coordinate system, defined in Fig. 1a as

$$\vec{V}_w = V_w \cos\gamma\, \vec{i} - V_w \sin\gamma\, \vec{j} \tag{1}$$

Transforming the rotor coordinate system in the blade coordinate system we have

$$\vec{V}_w = V_w \cos\gamma\, \vec{i}_1 - V_w \sin\gamma \cos\psi\, \vec{j}_1 + V_w \sin\gamma \sin\psi\, \vec{k}_1 \tag{2}$$

The rotational motion of the blade will add a velocity component Ωr in the direction $\vec{j}_1$, so that the total velocity vector relative to the blade, $\vec{W}$ is

$$\vec{W} = V_w \cos\gamma\, \vec{i}_1 + (\Omega r - V_w \sin\gamma \cos\psi)\, \vec{j}_1 + V_w \sin\gamma \sin\psi\, \vec{k}_1 \tag{3}$$

If the blade is additionally allowed to flap through angle β about y_1, then the total velocity vector $\vec{W}$ transformed into the final coordinate system, shown in Fig. 2, becomes

$$\vec{W} = (V_w \cos\gamma \cos\beta - V_w \sin\gamma \sin\psi \sin\beta)\vec{i}_2 + (\Omega r \cos\beta - V_w \sin\gamma \cos\psi)\vec{j}_2 + \\ + (V_w \sin\gamma \sin\psi \cos\beta + V_w \cos\gamma \sin\beta)\vec{k}_2 \tag{4}$$

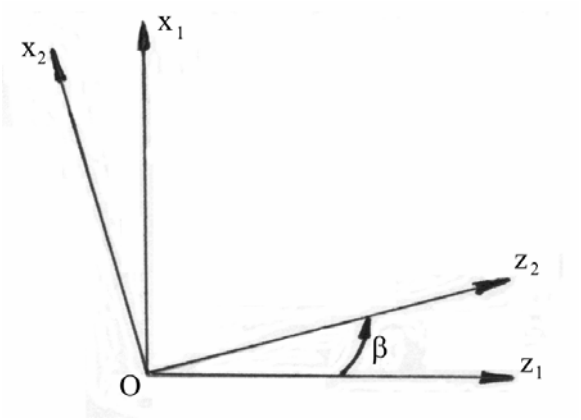

Fig. 2 Velocity profiles near wall.

The effects of the axially, radial and rotationally induced velocities can now be included giving the components of relative wind in the $\left(\vec{i}_2, \vec{j}_2, \vec{k}_2\right)$ coordinate system as

- normal to rotation plane and span

$$W_i = V_w \cos\gamma \cos\beta - v_a \cos\beta - \left(V_w \sin\gamma \sin\psi \sin\beta - v_a \tan\frac{\chi}{2}\sin\psi \sin\beta\right), \tag{5}$$

- chordwise

$$W_j = \Omega r \cos\beta + v_t - \left(V_w \sin\gamma \cos\psi - v_a \tan\frac{\chi}{2}\cos\psi\right) \tag{6}$$

- spanwise

$$W_k = V_w \sin\gamma \sin\psi \cos\beta - v_a \tan\frac{\chi}{2}\sin\psi \cos\beta + V_w \cos\gamma \sin\beta - v_a \sin\beta, \tag{7}$$

where χ is the wake skew angle.

Further on we define the non-dimensional velocities

$$a = \frac{v_a}{V_w \cos\gamma}, \qquad C_i = \frac{W_i}{V_w \cos\gamma},$$

$$a' = \frac{v_t}{\Omega r \cos\beta}, \qquad C_j = \frac{W_j}{V_w \cos\gamma},$$

$$\lambda = \frac{\Omega R \cos\beta}{V_w}, \qquad C_k = \frac{W_k}{V_w \cos\gamma},$$

$$X = \frac{\Omega r \cos\beta}{V_w},$$

and substitute them into equations (5-7) to obtain

$$C_i = (1-a)\cos\beta - \left(\tan\gamma - a\tan\frac{\chi}{2}\right)\sin\psi\sin\beta \tag{8}$$

$$C_j = \frac{X}{\cos\gamma}\left(1 + a' - \frac{\sin\gamma\cos\psi}{X} + \frac{a\cos\gamma\tan\frac{\chi}{2}\cos\psi}{X}\right), \tag{9}$$

$$C_k = tg\gamma\sin\psi\cos\beta - a\tan\frac{x}{2}\sin\psi\sin\beta + (1-a)\sin\beta \tag{10}$$

2.2 Aerodynamic Loads

The basic idea of BEM mode is to balance both the linear and singular momentum changes of the air masses flowing through the rotor disc with the axial force and torque generated on the rotor blades respectively. This balance is carried out in a detailed fashion, considering the flow through annular strips of width dr and the aerodynamic forces on blade elements of the same width; the forces are obtained from 2D wind tunnel data for the lift coefficient $C_L(\alpha)$ and the drag coefficient $C_D(\alpha)$. Both coefficients depend mainly on the angle of attack and Reynolds number.

By convention the modification of the wind velocity field (assumed to be uniform well ahead of the wind turbine) is expressed in terms of the so-called (axial and tangential) induction factors a and a' defined by $U_d = V_w(1-a)\cos\gamma$ and $V_d = \Omega r(1+a')$, where V_w is the incoming freestream velocity, U_d is the axial velocity component in the rotor plane, V_d is the tangential velocity component as experienced by the rotating blade element and Ω is the angular velocity of the rotor.

To obtain the induction factors a, a' it is necessary to equate momentum theory with blade element theory and make due allowance for any tip losses. By using an average for an annular ring the elemental values of axial force and moment integrated around the ring are:

$$dF_b = \int_0^{2\pi}\frac{1}{2}\rho W^2\sigma_r C_x\cos^2\beta r\,dr\,d\psi, \tag{11}$$

$$dM_b = \int_0^{2\pi}\frac{1}{2}\rho W^2\sigma_r C_y r^2\cos^2\beta\,dr\,d\psi \tag{12}$$

and from the momentum theory we also have

$$dF_m = \int_0^{2\pi} 2\rho V_W^2\cos^2\gamma a f(1-a)\cos^2\beta r\,dr\,d\psi \tag{13}$$

$$dM_m = \int_0^{2\pi} 2\rho V_W\cos\gamma a' f(1-a)\Omega r\cos^4\beta r^2 dr\,d\psi \tag{14}$$

where $C_x = C_L\cos\phi + C_D\sin\phi$, $C_y = C_L\sin\phi - C_D\sin\phi$, $\sigma_r = Bc/2\pi r\cos\beta$ is the solidity parameter, c is the chord length, B is the number of blades and f is the tip loss factor[1].

It has been assumed that any radial flow corresponding to Eq. (10) and the expansion of wake can be neglected and that the equation (8) the can be reduced to

$$C_i = (1-a)\cos\beta \tag{15}$$

The flow angle ϕ is then determined by the components of velocity C_i and C_j

$$tg\phi = \frac{(1-a)\cos\gamma\cos\beta}{X(1+a^{'}) + \cos\psi\cos\gamma\left(a\tan\frac{\chi}{2} - \tan\gamma\right)}. \tag{16}$$

Now equating equations (11), (13) and (12),-(14) we obtain

$$a(1-a) = \frac{\sigma_r}{8\pi f}\int_0^{2\pi}\frac{W^2}{V_W^2\cos^2\gamma}C_x d\psi\,, \tag{17}$$

$$a'(1-a) = \frac{\sigma_r}{8\pi f X}\frac{\cos\gamma}{\cos\beta}\int_0^{2\pi}\left(\frac{W^2}{V_W^2\cos^2\gamma}\right)C_y d\psi\,. \tag{18}$$

The non-dimensionalized resultant velocity relative to a blade element is given by

$$\frac{W^2}{V_W^2\cos^2\gamma} = \left[(1-a)\cos\beta\right]^2 + \left[\frac{X(1+a')}{\cos\gamma} + \cos\psi\left(a\tan\frac{\chi}{2} - \tan\gamma\right)\right]^2. \tag{19}$$

By means of the flow angle ϕ the equations (17) and (18) can be rewritten under the form:

$$\frac{a}{1-a} = \frac{\sigma_r\cos^2\beta}{8\pi f}\int_0^{2\pi}\frac{C_x}{\sin^2\phi}d\psi\,, \tag{17'}$$

$$\frac{a^{'}}{1-a^{'}} = \frac{\sigma_r}{8\pi f}\int_0^{2\pi}\frac{C_y}{\sin\phi\cos\phi\left[1 - \dfrac{\tan\phi\tan\gamma\cos\psi}{(1-a)\cos\beta}\right]}d\psi\,. \tag{18'}$$

Since the local flow angle ϕ (Eq. 16) depends itself on the (local) induction factors, equations (17) and (18) generally represent a coupled non-linear system of equations. Hence, to derive the factors a and a' an iterative process is needed, the integrals being determined numerically.

The theory supports only the determination of azimuthally averaged values of the flow induced velocities. Once the induction factors are known as a function of the radial variable r the power coefficient for the complete blade can be calculated from

$$C_P = 8\lambda^2\cos\gamma\int_0^1\left(\frac{r}{R}\right)^3 a'(1-a)\,d\left(\frac{r}{R}\right)$$

The elemental lift and drag forces per unit length are: $L = \frac{1}{2}\rho W^2 c C_L$ and $D = \frac{1}{2}\rho W^2 c C_D$, with W^2 given by Eq. (19).

2. 3 Results

Based on the preceding analysis, a computer programme has been developed to predict the forces and moments of a horizontal axis wind turbine in non-axial flow. The blade shape and airfoil characteristics of two rotor designs, which had been determined by a blade optimization routine [1], were used as input data. The two rotors were both of fixed pitch and two bladed configurations, one designed to operate at an optimum tip speed ratio of nine and the other of six.

Figures 3 and 4 show the maximum power coefficient and the optimum tip speed ratio as a function of yaw angle (γ), with zero coning angle $(\beta = 0)$. For both rotors the maximum power coefficients lie on a curve close $\cos\gamma$ cubed, while the tip speed ratio varies approximately as $\cos\gamma$.

Figures 5 and 6 show the torque about the yaw axis as a function of the tip speed ratio and yaw. A negative value of the torque (C_{MZ}) indicates that the operating turbine will veer in a direction which restores axial flow. Conversely a positive value will increase the yaw.

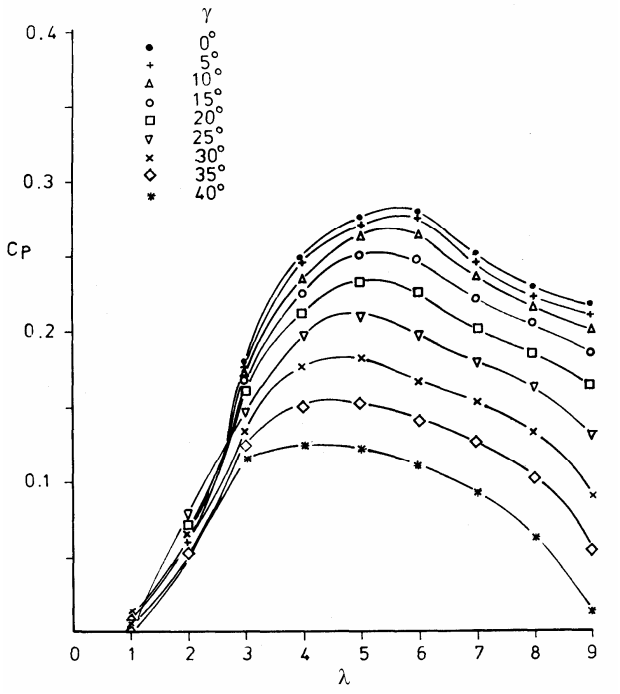

Fig. 3 Effect of yaw on the performance characteristic of a high speed rotor $(\lambda_{opt} = 9)$.

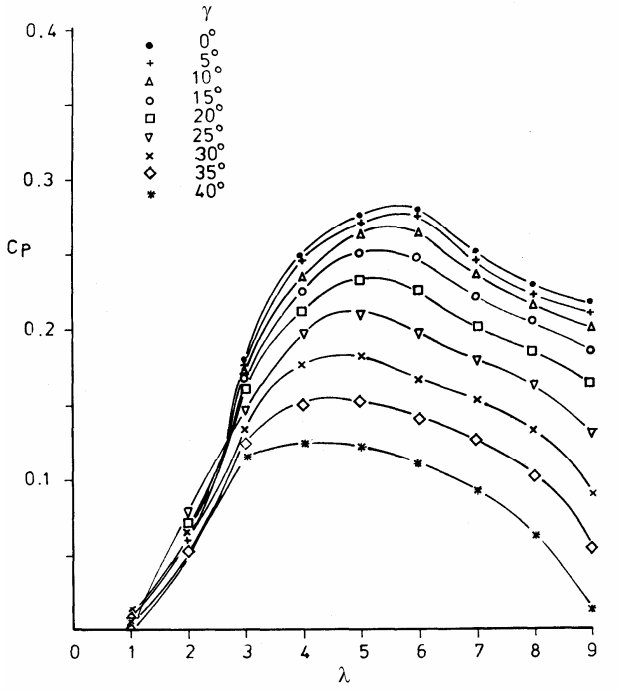

Fig. 4 Effect of yaw on the performance characteristic of a medium speed rotor $(\lambda_{opt} = 6)$.

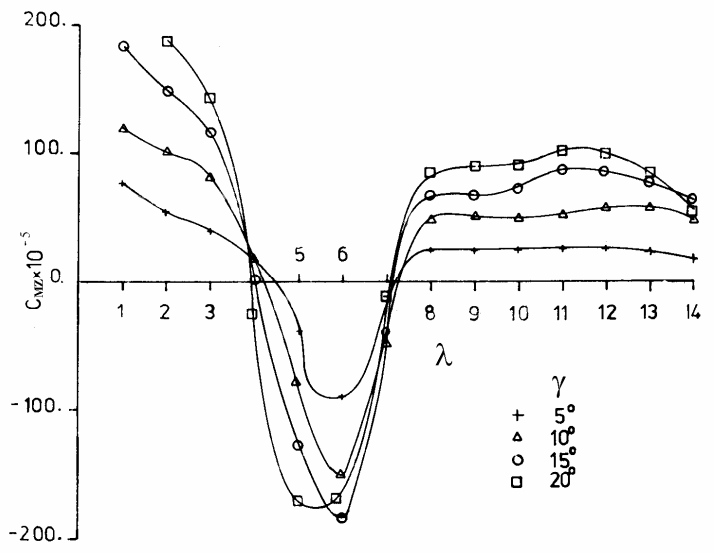

Fig. 5 Effect of yaw on the restoring torque $\left(\lambda_{opt} = 9\right)$.

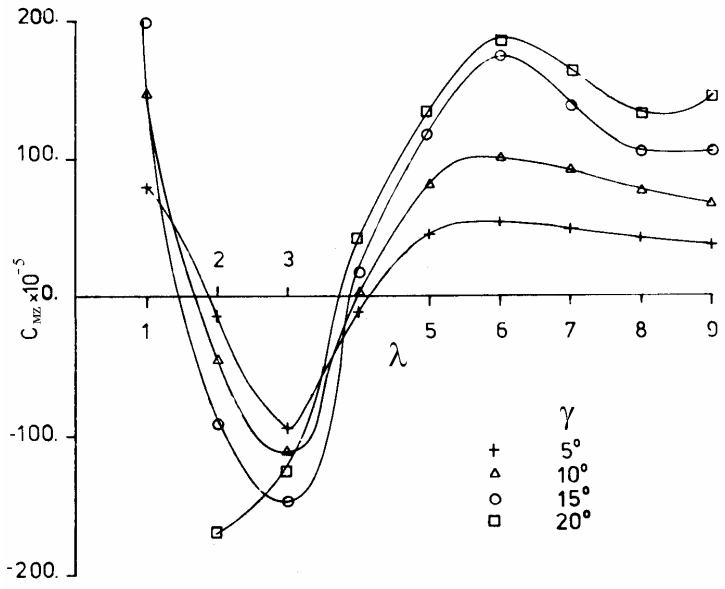

Fig. 6 Effect of yaw on the performance characteristic of a medium speed rotor $\left(\lambda_{opt} = 6\right)$.

3. AEROACOUSTIC ANALYSIS

The experimental results for a small teetered rotor wind turbine[4] revealed a 1/3 octave spectrum dominated by a broad peak in the higher frequency range at all yaw angles investigated. This has prompted the present theoretical investigation to reveal the mechanisms producing the dominant feature obtained in the experimental noise spectra.

The aerodynamic noise prediction method combines a model for predicting aerodynamic noise due to the effects of inflow turbulence upon on airfoil section, with prediction schemes for airfoil self-noise. The method is integrated into a program which averages the noise of the previous two bladed rotor our one revolution and gives as output a 1/3 octave, A-weighted spectrum at a user selectable location. Output

spectra are predicted at a downwind location for various yaw angles and comparisons with experiment are presented.

3.1 Inflow-Turbulence Noise

The wind turbine acts to transform incoming turbulence to radiated noise, which is potentially the most important source of aerodynamic noise from wind turbine at high wind speeds. The adopted prediction model for turbulence inflow noise is based on the semi-empirical model of Amiet[5] derived for a single airfoil section under turbulent inflow and extended to the case of rotating wind turbines by Lowson[6].

This model can be applied for both high and low frequency, with smooth transition between the two regions:

$$L_{P,INF} = L^{H}_{p,INF} + 10\log_{10}\frac{K_c}{1+K_c} \tag{20}$$

where $L^{H}_{p,INF}$ is the sound pressure level for high frequency region:

$$L_{P,INF} = 10\log_{10}\left[\rho_0^2 c_0^2 l \frac{\Delta s}{r^2} M^3 I^2 \hat{k}^3 \left(1+\hat{k}^2\right)^{-7/3}\right] + 58.4\,, \tag{21}$$

width l denotes the turbulence length scale and I denotes the turbulence intensity. Δs is the blade segment semi span (blade element width / 2) and r is the distance to the observer, measured perpendicular to the blade. The low frequency correction K_c in equation (20) is given as $K_c = 10S^2 M\hat{k}^2\beta^{-2}$, where S is a form of the compressible Sears' function, suggested by Amiet

$$S^2 = \left(\frac{2\pi\hat{k}}{\beta^2} + \frac{1}{1+2.4\hat{k}/\beta^2}\right)^{-1}, \text{ with } \beta^2 = 1-M^2.$$

The wave number is given by Lowson, corrected from Amiet, $\hat{k} = \pi f c / W$ and f is the 1/3 octave band center frequency.

3.2 Turbulent Boundary Layer – Trailing Edge Noise (TBL-TE)

As its name implies TBL-TE noise is caused by the flow of a turbulent boundary layer over the impedance discontinuity existing at the trailing edge of the airfoil. The effect of the edge is to radically increase the efficiency of the acoustic radiation of the turbulence, particularly at lower speeds. The scaling law applied is based on the result of Ffowcs Williams and Hall[7] for the problem of turbulence convecting past the trailing edge on a half-plane. The noise is described as a function of local Mach number *M*, displacement thickness, δ^* length of blade segment Δs, angle of attack α and the distance of the source to observer position r. The total sound pressure level, in 1/3 octave band, is given by Brooks, Pope, Marcolini model as:

$$L_{p,TBLTE} = 10\log_{10}\left\{10^{L_{p,\alpha}/10} + 10^{L_{p,s}/10} + 10^{L_{p,p}/10}\right\} \tag{22}$$

with

$$L_{p,\alpha} = 10\log_{10}\left(\frac{\delta_s^* M^5 \Delta s \overline{D}_h}{r^2}\right) + G_1\left(\frac{St_s}{St_2}\right) + K_1\,, \tag{23}$$

representing the effect of angle of attack

$$L_{p,s} = 10\log_{10}\left(\frac{\delta_s^* M^5 \Delta s \overline{D}_h}{r^2}\right) + G_2\left(\frac{St_s}{St_1}\right) + \left(K_2 - 3\right), \tag{24}$$

the contribution of the suction side and

$$L_{p,p} = 10\log_{10}\left(\frac{\delta_p^* M^5 \Delta s \overline{D}_h}{r^2}\right) + G_2\left(\frac{St_s}{St_1}\right) + \left(K_2 - 3\right) + \Delta K_2, \tag{25}$$

the contribution of the pressure side of the airfoil.

The Strouhal numbers are defined as: $St_s = f\delta_s^* / U, St_p = f\delta_p^* / U$. The high frequency directivity function $\left(\overline{D}_h\right)$, the empirical shape functions $\left(G_1, G_2\right)$, the amplitude functions $\left(K_1, K_2, \Delta K_2\right)$, and the peak Strouhal numbers $\left(St_1, St_2\right)$ are given in Brooks et al. [8].

Equations (23-25) are used if $\alpha \le \alpha_{ss}\left(= 12.5^0\right)$. At angles of attack above $\alpha_{ss}, L_{p,s}, L_{p,p} \to -\infty$ and the noise is totally dominated by separation-stall noise (Eq. 23).

3.3 Blunt-Trailing Edge Noise

Trailing edge bluntness on an airfoil can result in the shedding of vortices into the wake, similar to that observed behind cylinders. If its thickness is too large, then very high tonal noise may occur. The total sound pressure level caused by a blunt trailing edge is also modeled by a scaling law proposed by Brooks et al. [8].

$$L_{p,BTE} = 10\log_{10}\left(\frac{t^* M^{5.5} \Delta s \overline{D}_h}{r^2}\right) + G_3\left(\frac{t^*}{\delta_{avg}^*}, \psi_{TE}\right) + G_4\left(\frac{t^*}{\delta_{avg}^*}, \psi_{TE}, \frac{St'}{St'_{peak}}\right), \tag{26}$$

with the Strouhal number based on the trailing edge thickness t^*, $St' = ft^* / U$.

Comparisons with data for a flat plate revealed a dependence of the trailing edge angle ψ_{TE} of the airfoil on the sound pressure level. The empirical scaling function G_3 determines the peak level, and function G_4 represents the shape of the spectrum depending on Strouhal number and trailing edge angle. The average displacement thickness, $\delta_{avg}^* = \left(\delta_p^* + \delta_s^*\right)/2$, is determined from the values of suction and pressure side. The reference value of Strouhal number St'_{peak} is dependent on the ratio t^* / δ_{avg}^* and ψ_{TE} [8].

3.4 Results

In our present work, the aerodynamic program is coupled with the aerodynamic noise prediction model. For wind turbines operating at certain yaw angle, the velocity field is accurately computed taking into account the skew angle of vortex cylinder wake. Also, for each airfoil, the boundary layer displacement thicknesses are calculated at both pressure side and suction side using the airfoil code XFOIL [9]. Each blade segment is operating at different Reynolds number and angle of attack, so that an interpolation of the discreetly calculated boundary layer data.

The acoustic analysis is based on a 10 kW wind turbine for which some measurements have been performed in steady yaw state[4]. Some available descriptions are given in the following: rotor diameter: 7.62m; tower height:21.51m; blade number: 2; tip speed: 76 m/s; mean speed at hub height: 8.5 m/s; wind direction: upwind; receiver position: 30 m in downwind direction, at the ground level; ground surface roughness: $z_0 = 10mm$.

Figure 7 shows some results for inflow turbulence noise, for zero, 30 and 60 degree yaw angle. It is noted an increased sound pressure level by increasing the yaw angle. From Figure 8 the same tendency is observed for the total turbulent boundary layer-trailing edge noise for high frequency.

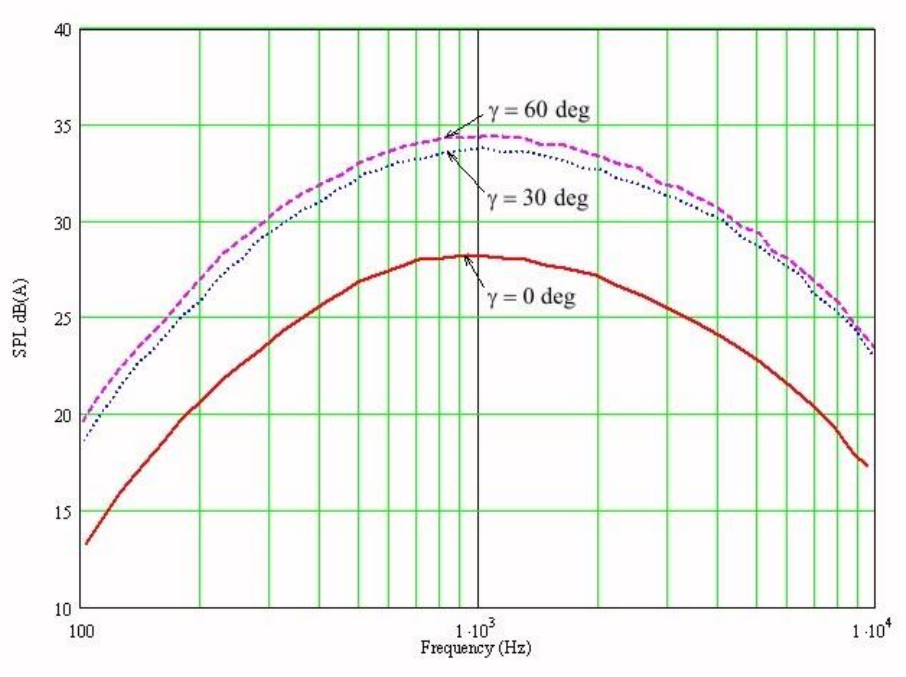

Fig. 7 Effect of yaw on the inflow turbulence noise.

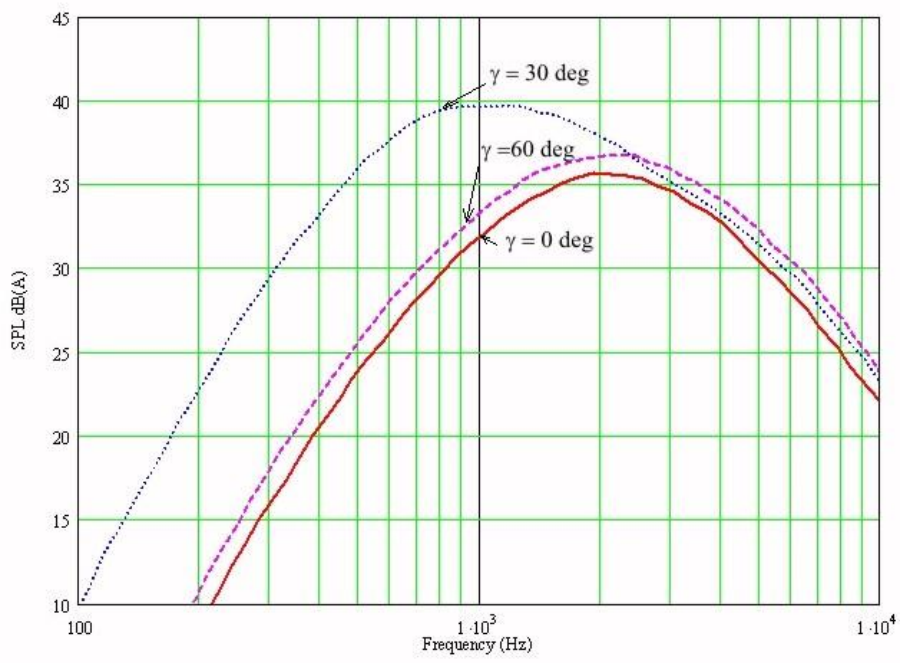

Fig. 8 Effect of yaw on the total turbulent boundary layer-trailing edge noise.

Results for the noise due to blunt trailing-edge are shown in Figure 9 for varying trailing-edge thickness and zero yaw angle. The trailing-edge bluntness adds a tonal component to the spectrum, its level depending on the thickness of the trailing edge. By reducing the thickness, the peak frequency is shifted towards higher frequencies and the level is reduced.

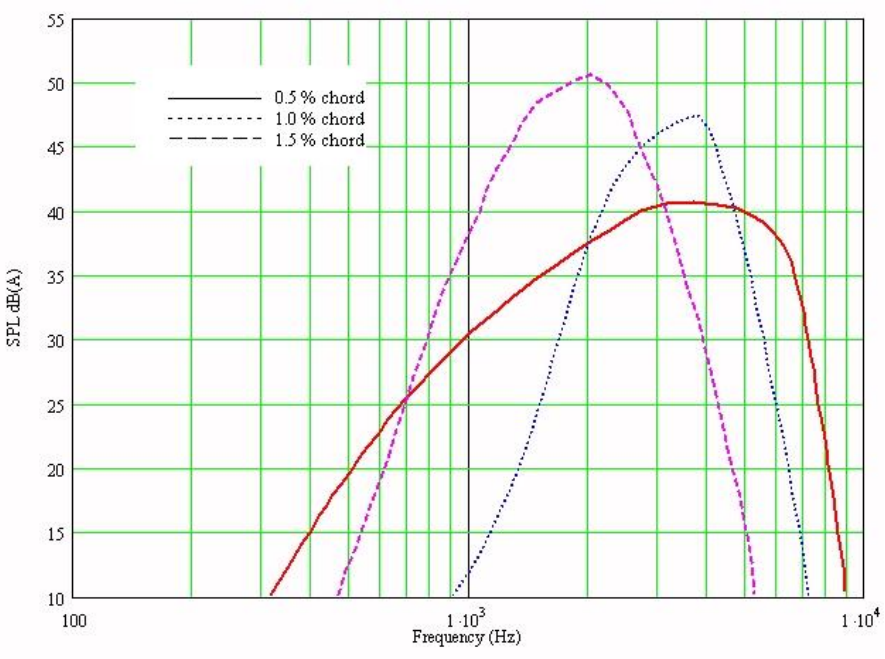

Fig. 9 Blunt trailing-edge noise for varying thickness.

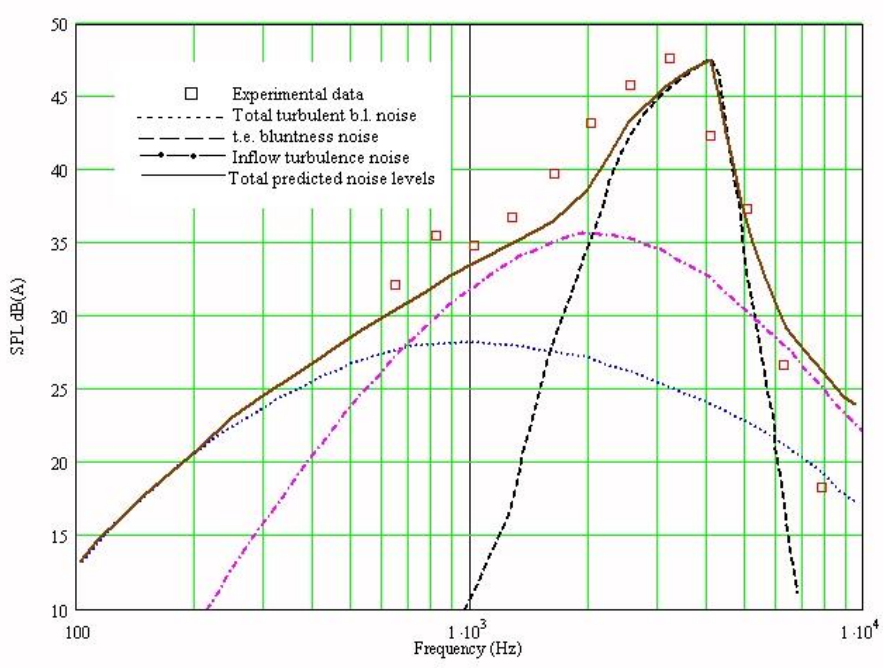

Fig. 10 Comparisons between total predicted noise levels and experimental data $(\gamma = 0\,\mathrm{deg})$.

The noise from all sources (INT, TBLTE, BTE) are plotted together with experimental data in Figures 10, 11 and 12 for three cases considered. These are representative of the noise generated at yaw angles of zero, 30 and 60 degrees. In all cases there is an overprediction of the noise levels at frequencies above 7000 Hz, probably due to the incomplete input data.

Figure 10 which depicts the zero yaw angle case, compares well with the numerical simulation except for a slight overprediction of the frequency of the peak sound pressure level. This is a direct consequence of the input values for the trailing edge thickness. A slightly larger value for this could lead to a closer match.

Figure 11, which depicts the 30 degree yaw angle case, also shows good agreement except for an isolated spike at 800 Hz, probably attributed to mechanical noise. Figure 12 shows that at yaw angles of 60 degrees and (probably) beyond the prediction starts to break down although the location of the trailing edge bluntness feature is still well captured. Reasons for this are expected to be associated with neglected blade wake interaction.

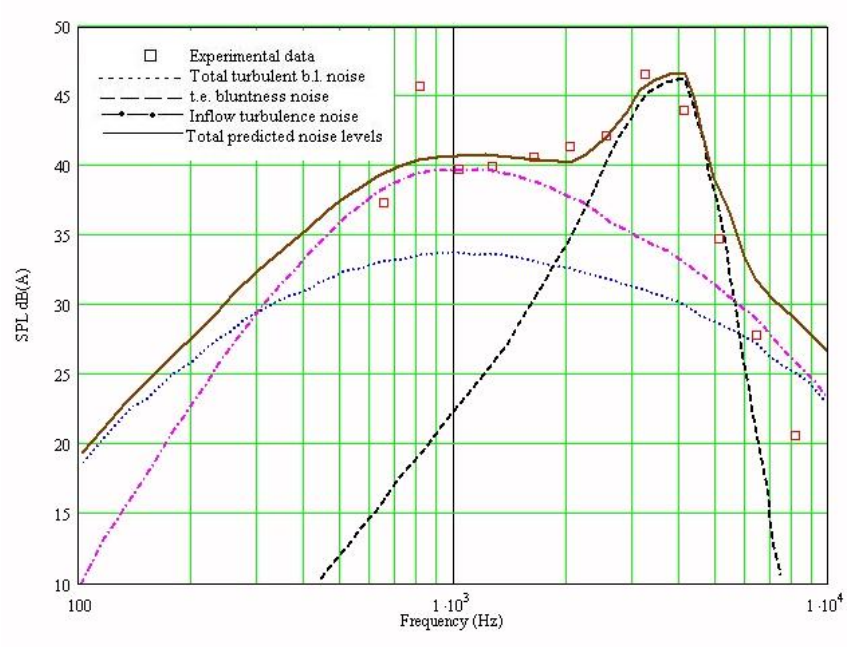

Fig. 11 Comparisons between total predicted noise levels and experimental data $(\gamma = 30\,\mathrm{deg})$.

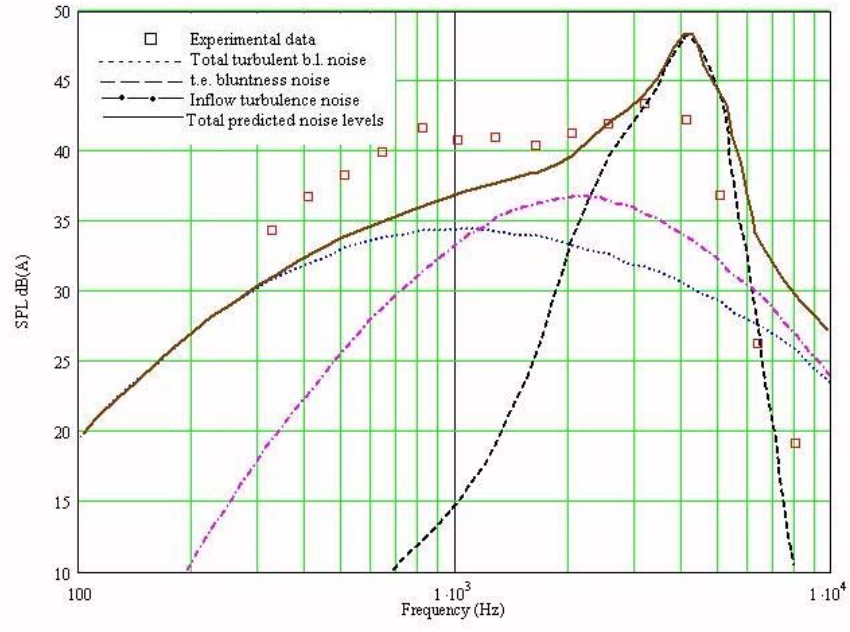

Fig. 12 Comparisons between total predicted noise levels and experimental data $(\gamma = 60\,\mathrm{deg})$.

4. CONCLUSIONS

In the present paper an aerodynamic BEM model and aeroacoustic method were developed to predict the power output and noise from a wind turbine rotor in yaw. The yawed rotor is less efficient than non-yawed rotor and so it is vital to assess the efficiency for purposes of energy production estimation and power control.

A theory based upon CFD should provide a much more accurate prediction of the aerodynamics of a wind turbine in yaw. However, the severe computational time limitations associated with CFD solutions preclude their use in favor of a simple theory like previously described.

The noise prediction model developed in conjunction with the aerodynamic model captures the key features of the noise produced by a wind turbine rotor in yaw. Some comparisons between predicted and experimental data show good agreement over all yaw angles up to 60 degrees. The model accurately predicts that the noise of the rotor is dominated by the tonal noise due to the trailing edge bluntness and this form of noise is controllable by simply sharpening of trailing edge.

REFERENCES

1. BURTON, T., SHARPE, D., JENKINS, N., BOSSANYI, E., *Wind Energy Handbook*, J. Wiley & Sons, Chichester, 2001.
2. DA SPERA (ed.), *Wind Turbine Technology: Fundamental Concepts of Wind Turbine Engineering*, ASME Press, New York, 1998.
3. HANSEN M., *Aerodynamics of Wind Turbines: Rotors, Loads and Structure*, James & James, London, 2000.
4. MOROZ, E. M., *Experimental and theoretical characterization of acoustic noise from a yaw controlled teetered rotor wind turbine*, UTEP, Master Thesis, 1995.
5. AMIET, R. K., *Acoustic radiation from an airfoil in a turbulent stream*, Journal of Sound and Vibration, 41, 4, 1975, pp. 407-420.
6. LOWSON, M.V., *Assessment and prediction of wind turbine noise*, ETSU W/13/00284/Rep. Harwell, England, 1993, pp. 1-46.
7. WILLIAMS FFOWCS, J.E., HALL, L., *Aerodynamic sound generation by turbulent flow in the vicinity of a scattered half plane*, *Journal of Fluid Mechanics*, 40, 4, 1970, pp. 657-670.
8. BROOKS, F.T., POPE, D.S., MARCOLINI, M.A., *Airfoil self-noise and prediction*, NASA RP-1218, 1989, pp. 1-137.
9. DRELA, M., XFOIL: *An analysis and design system for low Reynolds number airfoils*. Lecture notes in engineering low Reynolds number aerodynamics, Vol. 54, Springer-Verlag, New York, 1989.

Received November 12, 2007